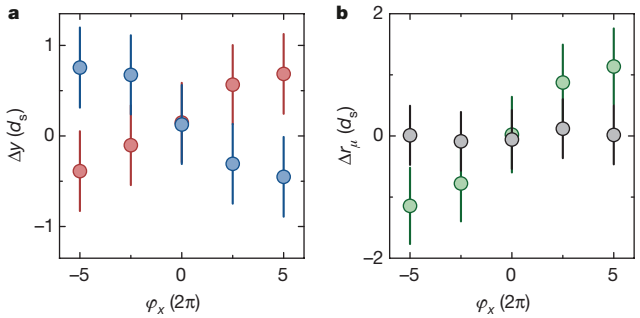

Figure 2 | 4D-like nonlinear centre-of-mass (COM) response. a, Shift in the COM of the cloud of atoms along y (Δy) versus the number of pump cycles along x (represented by φ_x) measured for two different angles, $\theta_1 = 0.78(2)$ mrad (red) and $\theta_2 = -0.85(2)$ mrad (blue), with $\varphi_y^{(0)} = 0.500(5)\pi$. When pumping along x, the cloud moves in the perpendicular y direction with the sign depending on the pumping direction and the sign of θ. Δy is the differential displacement for $V_{s,x} = 7.0(2)E_{r,s}$, $V_{s,y} = 17.0(5)E_{r,s}$, $V_{l,x} = 20.0(6)E_{r,l}$ and $V_{l,y} = 80(3)E_{r,l}$ compared to a reference sequence with $V_{s,y} = 40(1)E_{r,s}$ and $V_{l,y} = 0E_{r,l}$ (see Methods). Here $E_{r,i} = h^2/(8m_a d_i^2)$, with $i \in \{s, l\}$, denotes the corresponding recoil energy, with m_a the mass of an atom. Each point is averaged 100 times and the error bar takes into account the error of the mean as well as a systematic uncertainty of $\pm 0.3 d_s$. **b**, Difference in the COM drift between θ_1 and θ_2 for the x (grey) and y (green) directions: $\Delta r_\mu = \Delta\mu(\theta_1) - \Delta\mu(\theta_2)$, with $\mu \in \{x, y\}$. The direction of the nonlinear response reverses when changing the sign of θ, whereas the linear response is independent of θ. Data are calculated from the measurements in **a** (see Methods).

To quantify this nonlinear response, instead of *in situ* imaging we use site-resolved band mapping, which measures the number of atoms on even (N_e) and odd (N_o) sites along y. This method enables us to determine the average double-well imbalance, $\mathcal{I}_y = (N_o - N_e)/(N_o + N_e)$, accurately. If no transitions between neighbouring unit cells along y occur, then $\mathcal{I}_y$ is related directly to the COM motion (see Methods). An example measurement of $\mathcal{I}_y(\varphi_x)$ is shown in Fig. 3a. The measured nonlinear response is smaller than expected for an ideal system, owing to the appearance of doubly occupied plaquettes and band excitations along y during the pumping and to a finite pumping efficiency along x (see Methods). Taking these imperfections into account, we find excellent agreement between the experimental data and the expected imbalance (Fig. 3a). By performing a linear fit to the differential double-well imbalance $\mathcal{I}_y(\varphi_x) - \mathcal{I}_y(-\varphi_x)$, we extract the change in the population imbalance during one cycle, $\delta\mathcal{I}_y = \mathcal{I}_y(\varphi_x = 2\pi) - \mathcal{I}_y(\varphi_x = 0)$ (see Methods). For a homogeneously populated band, this slope is determined by $\overline{\Omega}$ and thus characterizes the transport properties of the system.

To reconstruct the quantized response of an infinite system and thereby obtain ν_2, we repeat the measurement of $\mathcal{I}_y(\varphi_x)$ for different $\varphi_y^{(0)}$ starting from the same initial position. This is equivalent to using the small cloud of atoms as a local probe at different positions along x for fixed $\varphi_y^{(0)}$ (Fig. 3b). To demonstrate the quantization of the nonlinear response, we determine the second Chern number of the lowest subband by averaging $\delta\mathcal{I}_y$ over $\varphi_y^{(0)} \in [0, 2\pi)$. For symmetry reasons, it is sufficient to restrict $\varphi_y^{(0)}$ to $[0, \pi)$ for $d_l = 2d_s$ (see Methods). In this interval, the nonlinear response has large contributions only in the vicinity of $\varphi_y^{(0)} = \pi/2$. For the range of data shown in Fig. 3c, this process gives $\nu_2^{\mathrm{exp}} = 0.8(2)$, with the error resulting from the fit and the uncertainty in θ. By taking the above-mentioned experimental imperfections into account we isolate the contribution from the lowest subband $\delta\mathcal{I}_y^{\mathrm{gs}}$ (see Methods). The experimentally determined slope of the nonlinear response for ground-state atoms agrees very well with the slope expected in an ideal system (Fig. 3c). To determine ν_2^{exp}, the ideal slope is fitted to the measured one by scaling it with a global amplitude, $(\nu_2^{\mathrm{exp}}/\nu_2)\delta\mathcal{I}_y^{\mathrm{gs}}(\varphi_y^{(0)})$. This yields $\nu_2^{\mathrm{exp}} = 1.07(8)$, in agreement with the expected value of $\nu_2 = +1$. The error in here additionally takes into account the uncertainties in the lattice depths.

In the 4D quantum Hall system, the defining feature of the nonlinear response is its linear dependence on the magnetic perturbation. The same scaling is thus expected for the 2D charge pump with respect to θ.

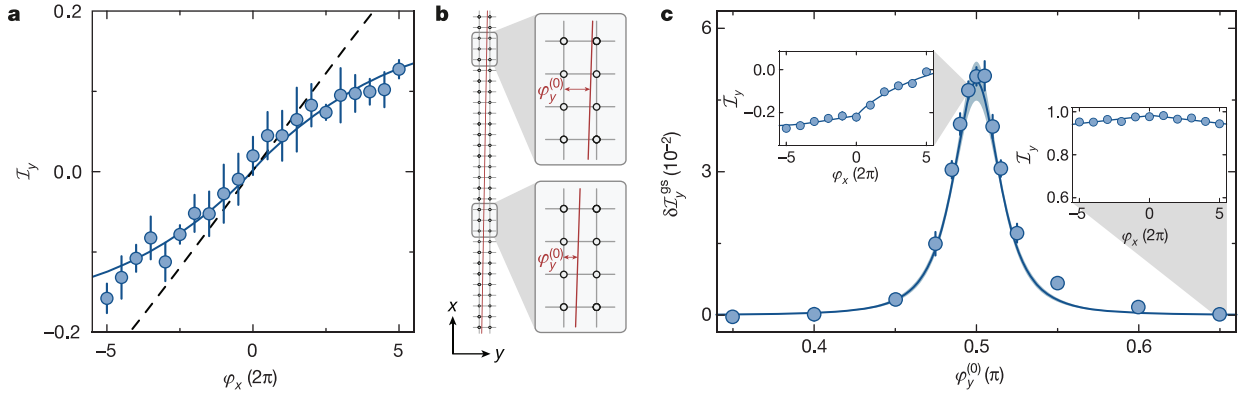

Figure 3 | Local probing of the quantized nonlinear bulk response for $\theta = 0.54(3)$ mrad. a, Double-well imbalance $\mathcal{I}_y$ versus the number of pump cycles in the x direction at $\varphi_y^{(0)} = 0.500(5)\pi$, $V_{s,x} = V_{s,y} = 7.0(2)E_{r,s}$ and $V_{l,x} = V_{l,y} = 20.0(6)E_{r,l}$. The data are the average of 14 measurements for the point at $\varphi_x = 0$ and 7 measurements for all others; the error is the error of the mean. The dashed line shows the response of an ideal system; the solid line includes corrections for the finite pumping efficiency along x and for the creation of doubly occupied plaquettes and band excitations along y. Both curves are shifted by a constant offset $\mathcal{I}_0 = 0.002$ (see Methods). For simplicity, the theoretical curves assume a homogeneous Berry curvature $\Omega^x = \nu_1^x a_x/(2\pi)$, neglecting the variation in Ω^x during a pump cycle. **b**, The response of an infinite system can be reconstructed with a small cloud of atoms by repeating the measurement from **a** for different values of $\varphi_y^{(0)}$. A single measurement probes the response locally at the position of the cloud (grey frames on the left). Changing $\varphi_y^{(0)}$ is equivalent to sampling a different position in the lattice (magnified frames on the right). Note that the tilt of the long y lattice (indicated by the red solid line, as in Fig. 1c) is greatly exaggerated compared to the angle used in the experiment. **c**, Change in the double-well imbalance per cycle for the lowest band ($\delta\mathcal{I}_y^{\mathrm{gs}}$) as a function of $\varphi_y^{(0)}$. $\delta\mathcal{I}_y^{\mathrm{gs}}$ is determined by the integrated Berry curvature $\overline{\Omega}(\varphi_y^{(0)})$ and so exhibits a pronounced peak around $\varphi_y^{(0)} = \pi/2$ (see Fig. 1e and Methods). The slope $\delta\mathcal{I}_y^{\mathrm{gs}}$ is extracted from a fit to the measured imbalance $\mathcal{I}_y(\varphi_x)$ (see Methods) and the solid line is the theoretically expected slope. Error bars show the fit error and the blue-shaded region indicates the uncertainty of the theoretical curve that results from the errors in θ and the lattice depths. The insets show two additional examples of individual measurements of $\mathcal{I}_y(\varphi_x)$ (for the values of $\varphi_y^{(0)}$ indicated by the grey shading), as in **a**.